Engineering 32 (2024) 174–185

Contents lists available at ScienceDirect

Engineering

journal homepage: www.elsevier.com/locate/eng

Research
Industrial Engineering—Article

A Resilience Approach for Diagnosing and Predicting HBV-Related Diseases Based on Blood Tests

Gege Hou [a,b], Yunru Chen [c], Xiaojing Liu [c], Dong Zhang [d], Zhimin Geng [d], Shubin Si [a,b,*]

[a] School of Mechanical Engineering, Northwestern Polytechnical University, Xi'an 710072, China
[b] Key Laboratory of Industrial Engineering and Intelligent Manufacturing (Ministry of Industry and Information Technology), Xi'an 710072, China
[c] Department of Infectious Diseases, The First Affiliated Hospital of Xi'an Jiaotong University, Xi'an 710061, China
[d] Department of Hepatobiliary Surgery, The First Affiliated Hospital of Xi'an Jiaotong University, Xi'an 710061, China

ARTICLE INFO

Article history:
Received 17 August 2022
Revised 14 December 2022
Accepted 1 June 2023
Available online 22 September 2023

Keywords:
HBV-related diseases
Functional resilience
Improve medical resource utilization
Critical states
Network

ABSTRACT

Chronic hepatitis B virus (HBV) infection, which threatens global public health, is a major contributor to liver-related morbidity and mortality. Examinations for liver diseases related to chronic HBV infection—including laboratory tests, ultrasounds, computed tomography (CT), and liver biopsies—may take up medical resources, particularly since they overlap in most instances. Thus, there is an urgent need to establish an economical and effective diagnosis method in order to streamline the medical process for HBV-related diseases. Using complex network models constructed based on clinical blood tests, we provide such a method by defining the novel measure of *functional resilience* to assess patients' liver conditions. By combining network models and dynamics, we discovered the pivotal items and their corresponding thresholds, which can guide further research on preventing disease deterioration in critical states of these diseases. The macro-averaged precision of our method, functional resilience, is 84.74%, whereas the macro-averaged precision of physicians' experience without assistance from imaging or biopsy is 55.63%. From an economic perspective, our approach could save the equivalent of at least 30 USD per visit for most Chinese patients and at least 400 USD per visit for most US patients, compared with general diagnostic methods. Globally, this will add to savings of at least 10.5 billion USD annually. Our method can comprehensively evaluate the condition of patients' livers and help avert the waste of medical resources during the diagnosis of liver disease by reducing excessive imaging exams.

1. Introduction

According to data from the World Health Organization [1], 350 million people currently have chronic hepatitis B virus (HBV) infection, 25%–40% of which will eventually die of various related conditions, such as liver cirrhosis (LC), acute-on-chronic liver failure (ACLF), or hepatocellular carcinoma (HCC). More than one million people die each year from HBV-related diseases. Up to two million Americans may have chronic infections, according to a recent report from the Institute of Medicine (IOM) on hepatitis and liver cancer, and up to 75% may be unaware of their infection status and show signs of late-stage disease [2]. The incidence of chronic HBV infection ranges from 2% to 7% in the Middle East and European nations. In the North and South American nations, the incidence of chronic HBV infection is less than 2%, whereas it exceeds 8% in African and Southeast Asian nations. In 2019, there were approximately 86 million patients with chronic HBV infection in China, with a high incidence of LC and liver cancer. Liver cancer is China's fifth most common cancer, accounting for 45% of all new cancer cases and 47% of liver cancer-related deaths worldwide. Therefore, the Chinese Center for Disease Control and Prevention has proposed active prevention, active detection, standardized treatment, and comprehensive control to address the harm caused by HBV, with the goal of eliminating HBV in China by 2030.

The costs associated with diagnosing and treating chronic HBV infection are high for both patients and healthcare systems [1,3,4]. More than one billion USD is spent annually on hospitalization costs for HBV-related patients in the United States. In 2012, the estimated annual direct medical expenses per patient at different stages of chronic HBV infection were 4098 USD in Iran [5]. In China, over 50 billion CNY is spent annually on hepatitis B diagnosis and treatment. Incomplete statistics indicate that 20% of these costs are related to over-examination, which has been a significant burden

* Corresponding author.
E-mail address: sisb@nwpu.edu.cn (S. Si).

https://doi.org/10.1016/j.eng.2023.06.013

to patients in terms of financial losses and complicated disease treatments. Moreover, physicians' inadequate levels of professional skills and experience may directly lead to misdiagnoses and delayed treatment [6,7].

At present, hepatitis B serological markers—namely, HBV DNA quantitative detection, serum alanine transaminase (ALT) concentration, and the aspartate aminotransferase (AST) to platelet (PLT) ratio index—are usually recommended to assess liver fibrosis [8,9], especially in low-resource settings. However, these markers are inadequate for comprehensively assessing liver function in the three states of chronic hepatitis B (CHB), LC, and HCC. Due to its limited sensitivity, serum alpha-fetoprotein (AFP) is no longer recommended for diagnosing HCC according to most international recommendations (indeed, in some guidelines, it is used in conjunction with radiological characteristics) [10]; however, it is still widely used in west Africa. Common imaging methods have disadvantages as well. Although ultrasound can dynamically reflect the blood supply characteristics of lesions in real time, there are some limits to ultrasound diagnosis, because the organs and gases in the abdomen can cause interference. In addition, sonographers' technical skills and personal judgment affect the accuracy of ultrasounds. Computed tomography (CT) can accurately assess the adjacent relationship between lesions and surrounding structures, but its radiation can accumulate and be harmful to patients, and its soft tissue resolution is low. Due to radiation absorption, physicians do not advise patients to undergo repeated CT scans in a short period of time. Magnetic resonance imaging (MRI) scans can satisfy multi-parameter and multi-directional imaging, and the use of hepatocyte-specific contrast agents can improve its detection rate and diagnostic accuracy in small HCC [11]. However, the drawback of MRI is that the patient-compliance requirements are relatively high, as the patient must remain in a fixed position for a specified amount of time. Moreover, there are shortages of MRI equipment and workforce in low- and middle-income countries, such as the eastern Mediterranean region, due to high costs [12]. Liver biopsy, another common diagnostic tool for liver disease, has possible complications, including pain and bruising at the biopsy site, bleeding for a long time, infection near the biopsy site, and accidental injury to another organ, especially for patients with advanced liver cancer who are not suitable for liver biopsy. To summarize, all the methods mentioned above may cause financial stress or physical harm to patients. Since blood tests are required for all patient visits, a comprehensive evaluation method that integrates blood test results is viable.

Numerous researchers have combined existing liver disease detection methods with machine learning algorithms to produce various liver disease diagnostic and prognostic models. Sazzadur et al. [13] developed an efficient diagnosis system for patients with chorionic liver infection using six distinct supervised machine learning classifiers. They studied the performance of all classifiers on patient information parameters and found that logistics regression (LR) provides the highest order precision of 75% based on the F1 measure to predict liver disease, while a naive Bayes (NB) classifier provides the lowest precision of 53%. Owjimehr et al. [14] presented an automatic region of interest (ROI) selection and hierarchical classification method to differentiate between a normal condition and the three stages of fatty liver—steatosis, fibrosis, and cirrhosis. Based on Raman spectral differences between healthy and hepatitis B-infected samples, Khan et al. [15] effectively separated normal and diseased serum using a support vector machine (SVM) algorithm, with a diagnostic accuracy of approximately 98% and a precision of approximately 97%. Deep learning radiomics of elastography (DLRE) [16] is a method for assessing hepatic fibrosis stages. In terms of predicting the stages of liver fibrosis, DLRE outperforms both two-dimensional shear wave elastography (2D-SWE) and biomarkers. However, distinguishing between the fibrosis stages F0–F1 and F2–F4 is relatively difficult for DLRE, due to the fact that the heterogeneity of liver fibrosis is more severe in > F2 than in $\geq$ F3 and F4, which decreases the accuracy of DLRE. Using a supervised machine-learning algorithm, Ye et al. [17] were the first to create a molecular signature capable of classifying metastatic HCC patients; they also identified genes relevant to metastasis and patient survival. The researchers found that osteopontin functions as both a diagnostic marker and a potential therapeutic target for metastatic HCC. Based on age, sex, clinical data, and blood biomarkers of HBV- and hepatitis C virus (HCV)-infected patients, Wong et al. [18] developed an HCC ridge score from a ridge regression model, which outperformed these common HCC risk scores in terms of a large area under the receiver operating characteristic curve (AUC ROC 0.840).

It is arduous to capture the critical reversible states at which the livers of patients exhibit fibrosis, precancerous lesions, or hepatocarcinogenesis due to chronic inflammation, since most patients have no symptoms during the early stage. Once patients progress to cirrhosis or HCC, it is difficult—even with close surveillance and treatment of these lesions—to improve survival rates. Although a concerted effort has been made to address the deterioration caused by liver diseases by studying antiviral medications [19–24] and pathogenic genes [25–31], these methods cannot provide early warning for physicians and patients. Thus, how can we infer whether patients are in a critical state from their basic clinical tests and provide criteria to alert physicians?

In this work, we utilize the correlation between clinical test items to develop complex network models for CHB, LC, and HCC (Fig. 1), because every patient must undergo a blood test when seeking medical care. From the perspective of a network, the liver function status in CHB, LC, and HCC can be clearly described. In addition, we provide the evolution dynamics of liver function and utilize analytical techniques to evaluate the liver function of patients. Our algorithmic approach leads to several key findings. After defining a new measure we term *functional resilience*, we find substantial variation in the functional resilience values of the CHB, LC, and HCC states, which can be employed to diagnose liver disease. The macro-averaged precision of our method based on functional resilience is 84.74%, whereas the macro-averaged precision of physicians' expertise without assistance from imaging and biopsy is 55.63%. The macro-averaged recall of our method is 84.39% compared with that of physicians, at 55.45%. To balance the impact of precision and recall, we use the F1-score to compare the effectiveness of the two methods. Our method yields an F1-score of 84.50%, which is substantially higher than that of physicians' expertise without imaging and biopsy assistance. Compared with other standard methods, functional resilience is affordable and will help physicians make clinical diagnoses, especially in medically under-equipped countries and areas such as the West Pacific region and Africa.

Another key finding of our work is that we can divide these items into several groups according to patient status by means of a community detection algorithm, rather than medical classification. This result reflects the fact that the liver's regulation function varies with disease progress. Furthermore, through simulation, we discover the critical conditions of state transition, including crucial items and their critical values. Once the test results surpass the corresponding conditions, patients may transition between phases, which is irreversible.

2. Material and methods

2.1. Sample collection

Data was provided by the Department of Infectious Diseases and Hepatobiliary Surgery, the First Affiliated Hospital of Xi'an Jiaotong

University, Xi'an, Shaanxi Province, China. We collected data from 119 patients with mild or moderate CHB stage, 175 patients with LC in either the compensated stage (10%; i.e., 17 patients in the compensated stage) or decompensated phase (90%; where 148 patients were in Child-Pugh class B and ten patients were in Child-Pugh class C) without hepatic encephalopathy, and 98 patients with HCC without metastasis (data is listed in Appendix A). The patients underwent six essential clinical trials when they first came to the hospital, including a complete blood count test, hepatitis B serologic test, HBV DNA quantitative detection, liver panel, blood clotting tests, and AFP tumor marker test. Here, it should be noted that we only considered four items of the hepatitis B serologic test—that is, hepatitis B surface antigen (HBsAg), hepatitis B surface antibody (HBsAb), hepatitis B e-antigen (HBeAg), and hepatitis B e-antibody (HBeAb), since the total hepatitis B core antibody is positive as long as people have been infected with HBV. More specifically, only 25 imperative items are considered in this article, and each item is divided into different levels according to the diagnostic criteria treatment guidelines for liver diseases [32–34] and the Child-Pugh score [35,36].

2.2. Functional network liver model

We assume that all patients whose data we collected are in stable states. The data can be converted to two or four values (Table S1 in Appendix A). Sequentially, the correlation coefficient between two clinical items (x_i, x_j) is calculated as follows:

$$\rho(x_i, x_j) = \frac{\mathrm{cov}(x_i, x_j)}{\sigma_{x_i}\sigma_{x_j}}$$

where $\mathrm{cov}(x_i, x_j)$ is the covariance between clinical items x_i and x_j, and σ_{x_i} and σ_{x_j} are the standard deviations of clinical items x_i and x_j, respectively. Therefore, the elements of the adjacency matrix A follow

$$A_{ij} = \begin{cases} 1, \text{if}\, \rho(x_i, x_j) \geq 0.25 \\ 0, \text{if}\, \rho(x_i, x_j) < 0.25 \end{cases}$$

That is, the edge exists when $A_{ij} = 1$; otherwise, it does not exist. Network models of CHB, LC, and HCC were built as shown in Figs. 1(b)–(d), respectively.

2.3. Dynamics model and phase transition

We found two types of relationships between the items of the tests: positive or negative correlation. If there is a positive correlation between two items, an increase in one item will increase the other. Conversely, if there is a negative correlation between two items, an increase in one item will stimulate a drop in the other. Given the positive and negative regulation relationships between each pair of items, we can use a differential equation to simulate dynamic changes between items. A neural network, as reported in Ref. [37], can be used to recognize underlying relationships in a set of data through a process that mimics the way the human brain operates. The mechanism of information transfer among artificial neurons, as proposed in Refs. [38] and [39], can be captured as follows:

$$\frac{\mathrm{d}x_i}{\mathrm{d}t} = I - \frac{x_i}{R} + \frac{J_1}{2}\sum_{j=1}^{N}\widehat{A}_{ij}\{1 + \tanh[n(x_j - a)]\} + \frac{J_2}{2}\sum_{j=1}^{N}\bar{A}_{ij}\{1 - \tanh[n(x_j - a)]\} \quad (1)$$

where a is the firing threshold, n pinpoints the slope of the sigmoid function, I is the basal activity, R is the inverse of the death rate, and J_1 and J_2 represent the excitation and inhibition strength, respectively. $\widehat{A}_{ij}$ and $\bar{A}_{ij}$ are the active and suppressive adjacency matrix of the neural network, respectively. Thus, the entire adjacency matrix can be written as follows:

$$A = \widehat{A} + \bar{A} \quad (2)$$

We borrowed the concept of the neural network and made a few changes to the dynamics, as follows:

$$\frac{\mathrm{d}x_i}{\mathrm{d}t} = I_i - \frac{x_i}{R_i} + \frac{J_1^i}{2}\sum_{j=1}^{N}\widehat{A}_{ij}\{1 + \tanh[n(x_j - a)]\} + \frac{J_2^i}{2}\sum_{j=1}^{N}\bar{A}_{ij}\{1 - \tanh[n(x_j - a)]\} \quad (3)$$

where I_i is the self-change of node i, R_i is the inverse of the proportion of node i returning to a normal range, and $\widehat{A}_{ij}$ and $\bar{A}_{ij}$ are the positive and negative adjacency matrices of the network, respectively. N is the number of nodes that are not isolated. J_1^i and J_2^i are the excitation and inhibition strengths of node i. However, I_i and R_i are unknown parameters and must be estimated.

$$J_1^i = \frac{\sum_{j=1}^{N}P_{ij}}{\sum_{i=1}^{N}\sum_{j=1}^{N}\widehat{A}_{ij}}, \quad J_2^i = \frac{\sum_{j=1}^{N}Q_{ij}}{\sum_{i=1}^{N}\sum_{j=1}^{N}\bar{A}_{ij}} \quad (4)$$

where P and Q are the positive and negative correlation matrices, respectively.

Replacing node j's value x_j with the sample average $\langle x\rangle$, Eq. (3) can be approximated as follows:

$$\begin{aligned}\frac{\mathrm{d}x_i}{\mathrm{d}t} &\approx I_i - \frac{x_i}{R_i} + \frac{J_1^i}{2}\sum_{j=1}^{N}\widehat{A}_{ij}\{1 + \tanh[n(\langle x\rangle - a)]\} + \frac{J_2^i}{2}\sum_{j=1}^{N}\bar{A}_{ij}\{1 - \tanh[n(\langle x\rangle - a)]\} \\ &= I_i - \frac{x_i}{R_i} + \frac{J_1^i}{2}s_i^+\{1 + \tanh[n(\langle x\rangle - a)]\} + \frac{J_2^i}{2}s_i^-\{1 - \tanh[n(\langle x\rangle - a)]\}\end{aligned} \quad (5)$$

where $s_i^+ = \sum_{j=1}^{N}\widehat{A}_{ij}$ and $s_i^- = \sum_{j=1}^{N}\bar{A}_{ij}$ are the positive and negative degrees of node i, respectively. The hyperbolic tangent function $\tanh(x)$ can be represented by the following:

$$\tanh(x) = \frac{\mathrm{e}^x - \mathrm{e}^{-x}}{\mathrm{e}^x + \mathrm{e}^{-x}} = \frac{2}{1 + \mathrm{e}^{-2x}} - 1 \quad (6)$$

Thus, Eq. (5) can be written as follows:

$$\frac{\mathrm{d}x_i}{\mathrm{d}t} = I_i - \frac{x_i}{R_i} + \frac{J_1^i \cdot s_i^+}{1 + \mathrm{e}^{-2n(\langle x\rangle - a)}} + \frac{J_2^i \cdot s_i^- \cdot \mathrm{e}^{-2n(\langle x\rangle - a)}}{1 + \mathrm{e}^{-2n(\langle x\rangle - a)}} \quad (7)$$

where we let

$$f(x_i, s_i^+, s_i^-) = I_i - \frac{x_i}{R_i} + \frac{J_1^i \cdot s_i^+}{1 + \mathrm{e}^{-2n(\langle x\rangle - a)}} + \frac{J_2^i \cdot s_i^- \cdot \mathrm{e}^{-2n(\langle x\rangle - a)}}{1 + \mathrm{e}^{-2n(\langle x\rangle - a)}} \quad (8)$$

When the system reaches a steady state, Eq. (8) must satisfy

$$f(x_i, s_i^+, s_i^-) = 0 \quad (9)$$

From Eq. (9), the steady activity of an item i is

$$x_i = I_i R_i + R_i \cdot \left[\frac{J_1^i \cdot s_i^+}{1 + \mathrm{e}^{-2n(\langle x\rangle - a)}} + \frac{J_2^i \cdot s_i^- \cdot \mathrm{e}^{-2n(\langle x\rangle - a)}}{1 + \mathrm{e}^{-2n(\langle x\rangle - a)}}\right] \quad (10)$$

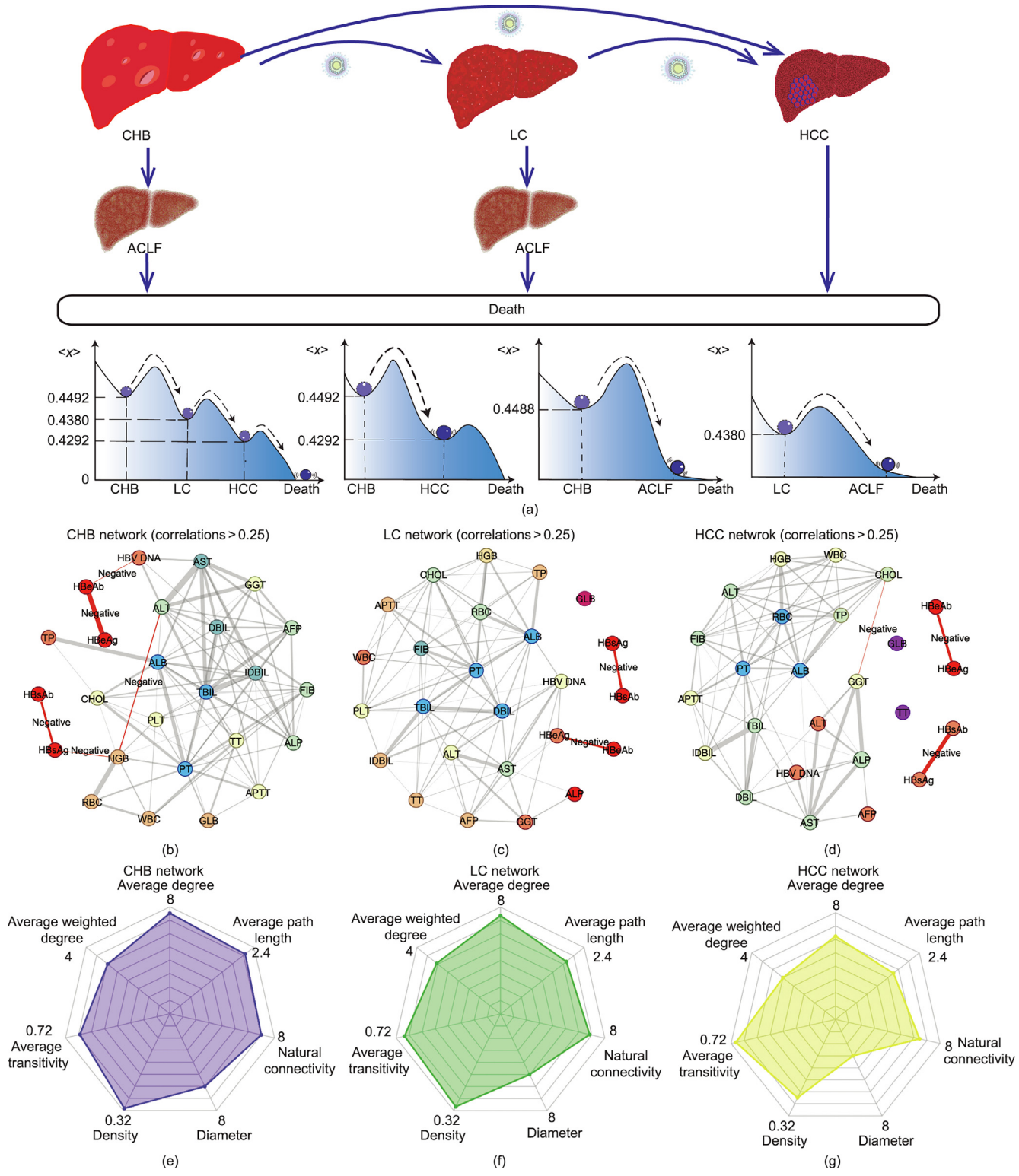

Fig. 1. Disease development and network structure of CHB, LC, and HCC. (a) Phase transition diagrams between CHB, LC, and HCC due to chronic HBV infection, including the situation of ACLF and death from HCC. Each blue ball represents a patient with the corresponding liver disease. When the ball crosses the peak, the patient undergoes a phase transition to the next state. Functional resilience in the three states is calculated by $\langle x_k \rangle = \frac{1}{N_k}\sum_{i=1}^{N_k} \exp\left\{-\frac{x_i^k \cdot 4}{\langle s_k \rangle}\right\}$, where $k = 1, 2, 3$ corresponds to the three states (i.e., CHB, LC, and HCC, respectively), $\langle s_k \rangle$ is the mean degree of the network in the state k, and N_k is the number of the non-isolated items in state k. (b–d) Networks of the clinical test items of CHB, LC, and HCC are constructed. Different colors of the nodes represent their degrees, and the link thickness indicates the strength of the correlations between items. Red lines indicate a negative correlation between items. (e–g) Three radar charts illustrating the topology structure of the corresponding networks.

Since the limit $\lim_{n\to\infty} e^{-2n(\langle x\rangle - a)} = 0$, Eq. (10) can be approximated as follows:

$$x_i = I_i R_i + R_i \cdot J_1^i \cdot s_i^+ \tag{11}$$

The proportion of edges that represent negative correlations between nodes, p, can be denoted as follows:

$$p = \frac{\sum_{i=1}^{N}\sum_{j=1}^{N}\bar{A}_{ij}}{\sum_{i=1}^{N}\sum_{j=1}^{N}A_{ij}} = \frac{\sum_{i=1}^{N}\sum_{j=1}^{N}\bar{A}_{ij}}{\sum_{i=1}^{N}\sum_{j=1}^{N}\left(\widehat{A}_{ij}+\bar{A}_{ij}\right)} \tag{12}$$

Since the sample mean $\langle x\rangle = \frac{1}{N}\sum_{i=1}^{N} x_i$, we recouple Eq. (3) into one dimension based on Eqs. (4), (11), and (12):

$$\langle x\rangle = I_i R_i + R_i \cdot J_1' \cdot \langle s\rangle \cdot (1-p) \tag{13}$$

where $J_1^i = \frac{\sum_{i=1}^{N}\sum_{j=1}^{N} P_{ij}}{\sum_{i=1}^{N}\sum_{j=1}^{N}\widehat{A}_{ij}}$ is the excitation strength of a network, and $\langle s\rangle = \frac{\sum_{i=1}^{N}\sum_{j=1}^{N}\left(\widehat{A}_{ij}+\bar{A}_{ij}\right)}{N}$ is the average degree of a network without isolated nodes. Hence, setting $n=2$ and $a=-1$, the unknown parameters I_i and R_i are obtained by solving Eqs. (11) and (13) simultaneously.

3. Results

3.1. Network construction and topology structure

Phase transition diagrams between CHB, LC, and HCC due to chronic HBV infection was shown in Fig. 1(a). According to the correlation of the blood parameters, we constructed the networks depicted in Figs. 1(b)–(d) for CHB, LC, and HCC. In these three diseases, the network densities are 0.3133, 0.3067, and 0.2533, respectively. It is clear that the more severe the liver damage is, the sparser the networks are. As the disease progresses, abnormal liver tissues such as scars and cancer cells progressively supplant normal liver cells, and the remaining normal cells are unable to perform their original functions, resulting in a decline in liver function and a subsequent impact on other body functions. As a result, the correlation between the respective blood indicators decreases, leading to the disappearance of the connecting boundaries between indicators. Using CHB as an illustration, the HBV primarily causes inflammation in the patient's liver. Therefore, inflammation-related edges exist in the CHB network, such as the edge between ALT and alkaline phosphatase (ALP). However, these connected edges are absent from the LC network. This is due to the fact that, in the cirrhosis state, liver inflammation is no longer the primary cause of the deterioration of the patient's condition; rather, the cause is the progressive replacement of normal liver cells with lesions, which are unable to maintain the various functions of the liver. A comparison of the edges in the three networks shows that the negative correlations colored in red between the items of hepatitis B serology gradually lose connections with the other items as the liver disease progresses. This means that hepatitis B serology loses its referential importance in the LC and HCC states. Similarly, globulins (GLB) and thrombin time (TT) are isolated in the LC and HCC states.

The proportions of the three radar charts also reflect the topological properties of the CHB, LC, and HCC networks (Figs. 1(e)–(g)). In the CHB state, the average transitivity of the network is 0.6114 and the average path length is 2.1533, which shows small-worldness. Similar to the CHB network, the LC network has a small-world property, since its average transitivity and the average path length are 0.7298 and 1.8961, respectively. Small-worldness also appears in the HCC network, but its average transitivity and average path length are less than those of the other two diseases. Therefore, as patients' liver disease develops from CHB to LC, and then to HCC, the average path length decreases, and the networks gradually become sparse. This is because, as the disease worsens, the correlation between the items of medical tests gradually weakens and the links are lost. Moreover, the links in the different networks appear, disappear, and reappear as the liver function deteriorates. For example, the nine edges of the CHB network related to three parameters, ALT, ALP, and gamma-glutamyl transferase (GGT), do not exist in the LC network but reappear in the HCC network. The reason for this phenomenon is that persistent inflammation promotes cancer cell production by suppressing immunosurveillance [40]. The specific changes are shown in Tables S2 and S3 in Appendix A.

Finally, considering the degree of liver damage due to HBV infection in the different states, we employed natural connectivity [41] as a measurement to simulate an item losing correlations with the other items. The result shows that, no matter how many items become independent, the natural connectivity of the CHB network is higher than those of the other two networks, while that of the HCC network is the lowest. Hence, the network in the CHB state is the most robust, whereas the HCC state has the most fragile network (Section S1.4 in Appendix A).

3.2. Community detection

Usually, items from distinct clinical tests are separated into several groups based on their functions. For example, AST, ALT, ALP, and GGT reflect the severity of liver damage. The serum bilirubin level, including the total bilirubin (TBIL), direct bilirubin (DBIL), and indirect bilirubin (IDBIL), shows a liver's catabolism. The total protein test and blood clotting test measure a synthesis function of the liver. Unlike the medical classification, we divide these items according to different states by means of a community detection algorithm, Infomap [42,43], which is one of the most effective algorithms among non-overlapping community discovery problems. In the CHB state, all the tests except hepatitis B serology belong to the same group, since hepatic inflammation leads to coagulation disorders and abnormal blood cells with the increase of serum HBV DNA concentration, such that the items have a strong correlation within this community (Fig. 2(a)). Moreover, the four items of hepatitis B serology split naturally into two small communities according to their name and interpretation. Conversely, the largest community in the CHB network is divided into two groups in the LC and HCC networks (Figs. 2(b) and (c)). Compared with their correlation with other items, there are close bonds among HBV DNA, the items measuring liver inflammation, and the liver tumor marker AFP. This is because the continuous replication of HBV and the inefficiency of the long-term antiviral treatments may eventually induce HCC. The remaining nodes in the red circle—except for isolated nodes and modules—display the liver's regulation function.

3.3. Dynamics and network resilience

It is well known that the disease course of chronic HBV infection involves a dynamic interaction between the virus and the host's self-regulation, which can be represented by changes in the liver function. For example, as HBV continuously attacks a patient's liver, abnormal liver function results in prolonged clotting time, leading to disorder of the coagulation system. In the state k, due to the correlation between the nodes' behavioral value, x_i^k, and the network average degree $\langle s_k\rangle$, we transformed a behavioral value into

$$x'_{i,k} = e^{-\frac{4x_i^k}{\langle s_k\rangle}} \tag{14}$$

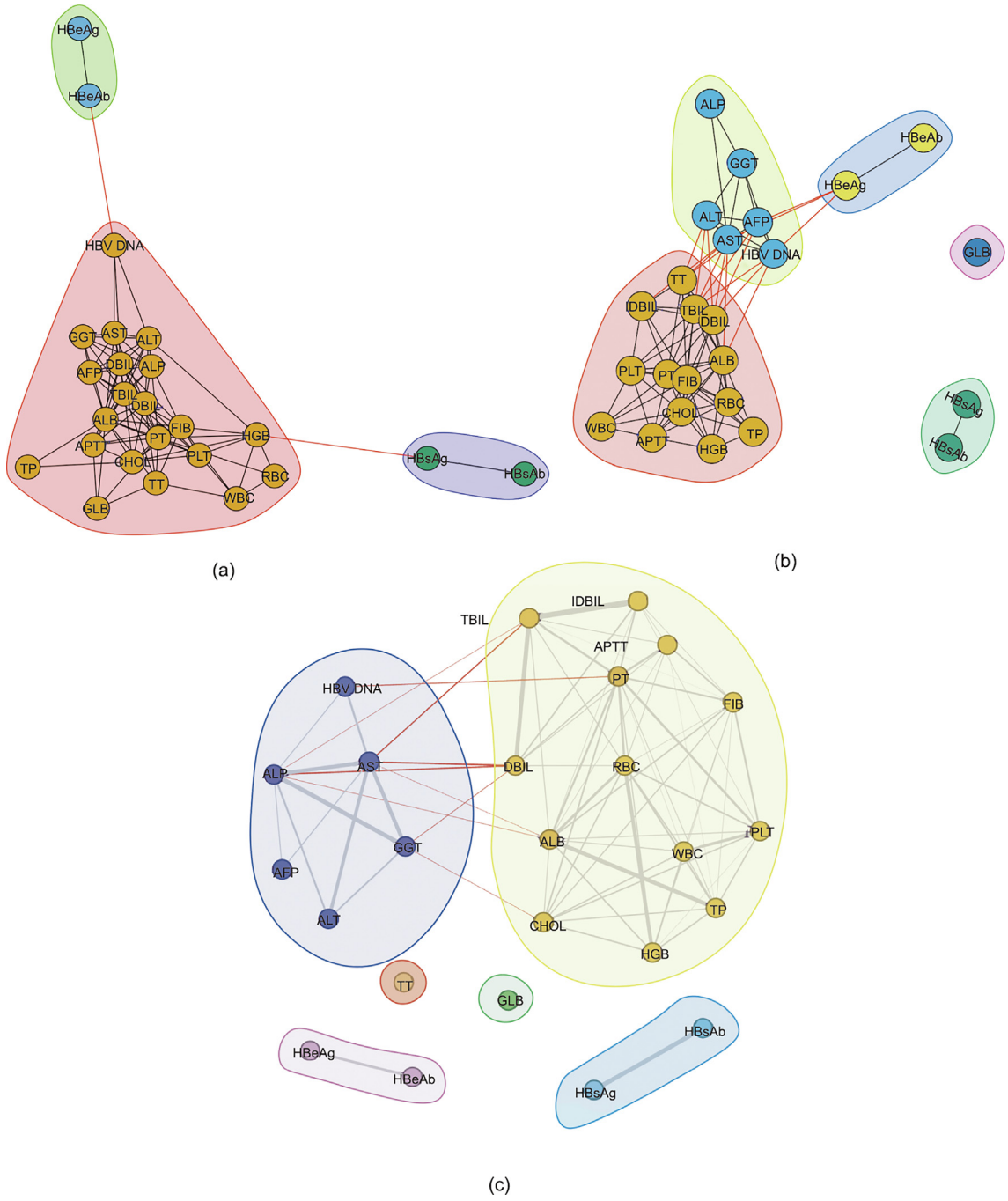

Fig. 2. The non-overlapping community structure in the networks of (a) CHB, (b) LC, and (c) HCC. Different colors of circles in each graph represent different communities. Red lines display the edges between communities, and black lines show connections between items in the same community. ALB: albumin; FIB: fibrinogen; APTT: thromboplastin time; PT: prothrombin time; CHOL: cholesterol; WBC: white blood cell; RBC: red blood cell; HGB: hemoglobin.

where $k = 1, 2, 3$ corresponds to the three states (i.e., CHB, LC, and HCC). Due to the correlation between blood test items, an increase in one indicator may result in an increase or decrease in the associated indicators. In the immune clearance or inactive carrier phase of CHB, the patient's HBeAg is positive, HBV replication is active, HBV DNA levels rise, and HBeAb is negative. Hepatitis B patients in remission have positive HBeAb, diminished HBV duplication, decreased HBV DNA, and negative HBeAg. Consequently, HBeAb has a negative relationship with HBeAg and HBV DNA concentration in the CHB network. Following the method introduced by Barzel et al. [44], we compared various dynamic models with positive and negative couplings. We found that the fitting error of the neural network dynamics was the smallest. Neuronal connections are modeled in neural networks as weights between nodes, as is well known. A positive weight represents an excitatory connection, while a negative weight represents an inhibitory connection. The error tolerance of neural networks ensures that the correct output can be obtained even if the input samples are inadequate or corrupted. Based on their interconnected structure and connection strength, neural network dynamics [38,39] simulate the process of information transmission between neurons. Using neural network dynamics, Baumann et al. [45] simulated reverberation effects and polarization phenomena in social networks.

Therefore, we consider each test item to be a neuron in a neural network, and each item correlation to be the excitation or inhibition regulation between neurons. In reality, the influence of each

item on the others varies, so we assume that the parameters I, R, J_1, and J_2 do not assume the same value during the fitting procedure. The equation can be rewritten as follows:

$$\frac{\mathrm{d}x'_{i,k}}{\mathrm{d}t} = I_{i,k} - \frac{x'_{i,k}}{R_{i,k}} + \frac{J_1^{i,k}}{2}\sum_{j=1}^{N_k}\hat{A}_{ij}^{k}\left\{1+\tanh\left[n\left(x'_{j,k}-a\right)\right]\right\} + \frac{J_2^{i,k}}{2}\sum_{j=1}^{N_k}\bar{A}_{ij}^{k}\left\{1+\tanh\left[n\left(x'_{j,k}-a\right)\right]\right\} \quad (15)$$

where N_k is the number of nodes in state k, $I_{i,k}$ and $R_{i,k}$ are the parameters that must be estimated in state k, $J_1^{i,k}$ and $J_2^{i,k}$ are the excitation and inhibition strength of node i in state k, and $\hat{A}_{ij}^{k}$ and $\bar{A}_{ij}^{k}$ are the corresponding matrices in state k. Substituting $I_{i,k}$ and $R_{i,k}$ into Eq. (3), we fitted the CHB, LC, and HCC networks with these dynamics, to simulate the regulatory interactions between items. Naturally, an item should not interact with any other item and should be deleted if it has no correlation with the others. Therefore, the items HBsAg, HBsAb, and GLB are deleted from the LC network, since they are dependent on the other items. Similarly, HBsAg, HBsAb, HBeAg, HBeAb, GLB, and TT are removed from the HCC network. According to the patients' clinical trial results and the transformation of the data, we fitted the CHB, LC, and HCC networks with these dynamics, to simulate the regulatory interactions between items. The deviation between each item's mean and simulated value is shown as follows. For the CHB, LC, and HCC networks, the sums of the absolute deviation of the fittings are 0.7440, 0.8120, and 0.5136, respectively. The fitting errors for each item in different states are minor and acceptable (Figs. 3(a)–(c)). This dynamics model fits these three networks ideally, so it can be assumed to align with the HBV "attack" dynamics.

Consider two types of perturbations that simulate loss and weakness of correlation between items owing to persistent chronic HBV infection. At first, we randomly removed edges from the networks (Fig. 3(d)), where the removal proportion is f_l and found that for a small proportion f_l of link removal, the three systems still maintain their resilience: each of them is stable at a corresponding fixed point x_H, in which the average score of all the items, $\langle x\rangle$, is high. However, when the perturbation exceeds a certain threshold the straight line disappears suddenly, resulting in two stable fixed points: the desired x_H and an undesired state x_L (Figs. 3(e)–(g)). Under these conditions the three systems lose their resilience, potentially transitioning to the undesired terminal stage. However, the thresholds of the link perturbation intensity for the CHB, LC and HCC networks are dissimilar, which means that the higher the threshold of link loss is, the more resilient the network is. Therefore, the CHB network is the most resilient when HBV attacks patients' livers since it remains resilient even after removing 85% of its links. Conversely, losing no more than 80% of its links will cause the HCC network to collapse. That is, the livers of patients are completely dysfunctional in the terminal stage. As for global weight loss, we decreased all weights on average to a fraction f_w of their original value (Fig. 3(h)). Then the resilience of the three

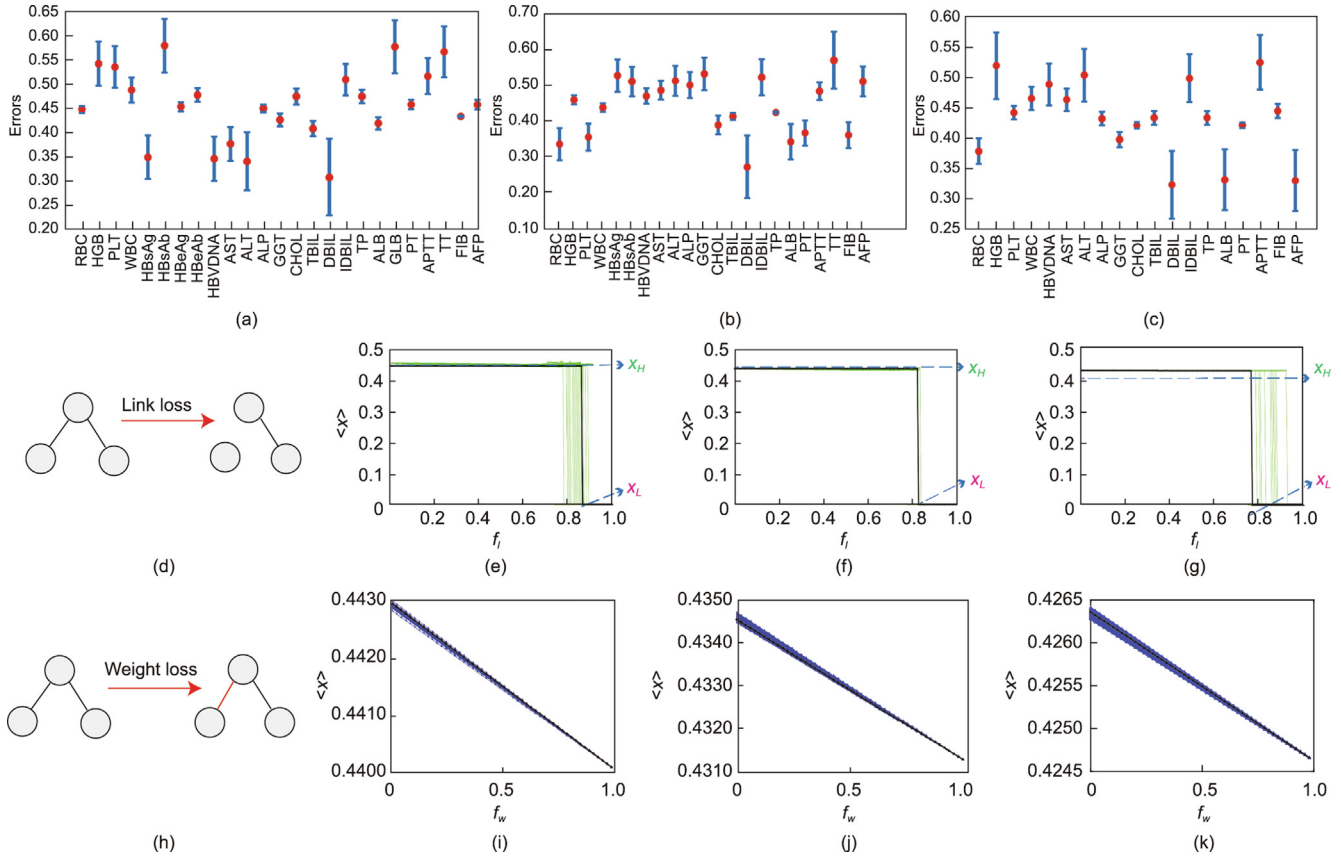

Fig. 3. Dynamics fitting and network resilience in the (a) CHB, (b) LC, and (c) HCC states. We fitted dynamics and estimated the unknown parameters $I_{i,k}$ and $R_{i,k}$ for (a) CHB, (b) LC, and (c) HCC, when the parameters $n = 2$ and $a = -1$. Red dots indicate the real values of the items, and blue lines show the fitted errors. (d) We tested the resilience of networks against the random disappearance of correlations with a proportion f_l. (e) Average levels of test items in the CHB network vs f_l across 100 realizations (we highlight the analytical solution in black). At a critical fraction f_l^c, the system undergoes a vertical drop, where, in addition to the desired state (x_H), an undesired state (x_L) emerges. (f, g) Similar results are observed in the LC and HCC networks. (h) We tested the resilience of networks against decreasing correlations on average to a fraction f_w of their original value, simulating a global change in the physical conditions of patients. (i) Similar simulations characterize the system's response to global perturbations f_w. (j) In the LC state, even if physicians perform antiviral treatment on patients, the condition will still deteriorate. (k) Similarly, the efficiency of antiviral treatment for patients with HCC is minimal.

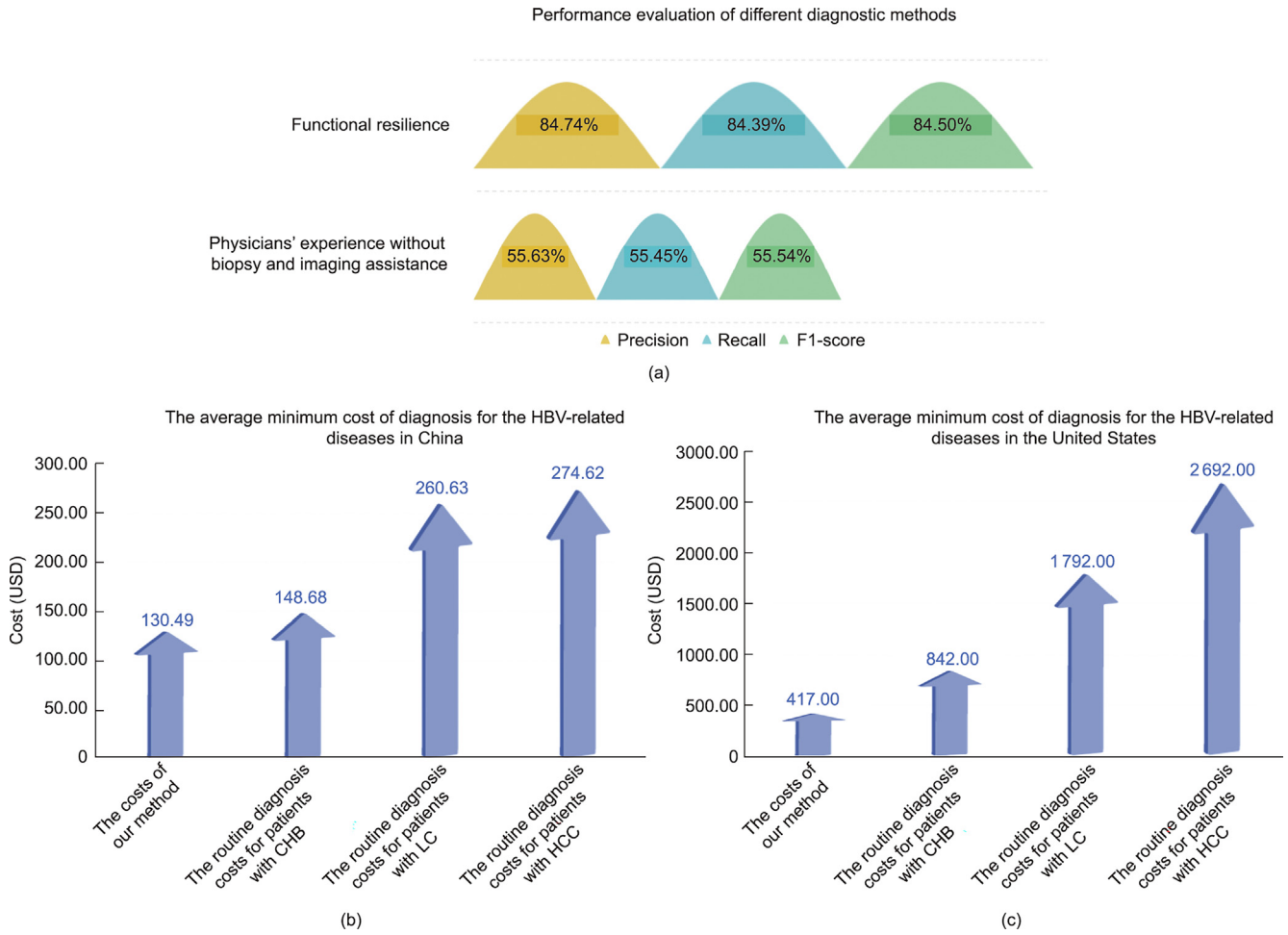

Fig. 4. A comparison of the efficacy and total cost of different diagnosis methods. (a) Comparison of the precision, recall, and F1-scores of functional resilience vs physicians' experience without assistance from imaging or biopsy. (b, c) Average minimum cost of different diagnosis processes for HBV-related diseases in China and the United States.

Table 1
Prices for typical clinical examination methods in China and the United States.

Examination method	Price in China (USD)	Price in the United States (USD)
Complete blood count test	4.20–11.19	10–39
Liver panel	13.99–27.99	49–79
Blood clotting tests	13.99–27.99	7–200
HBV DNA quantitative detection	13.99–83.96	16–232
Hepatitis B serologic test	3.50–41.98	11–90
AFP tumor marker test	4.20–13.99	16–85
Ultrasound for liver	8.40–27.99	200–650+
CT examination	No less than 41.98	No less than 350
MRI examination	No less than 69.97	No less than 600
Liver biopsy	No less than 83.96	No less than 1500

networks is gradually declining and then lost with strengthening perturbations (Figs. 3(i)–(k)). In contrast to link loss, the process of global weight reduction lacks intermediate fixed spots. In other words, even if HBV ceaselessly undermines liver cells but do not cause edges to break, patients still die from complete hepatic dysfunction.

3.4. Validity and cost-efficiency of functional resilience

The mean of the behavioral values in different states, which we term *functional resilience*, is defined as follows:

$$\langle x_k \rangle = \frac{1}{N_k} \sum_{i=1}^{N_k} x'_{i,k} \tag{16}$$

Similar to the Child-Pugh score, Eq. (16) can be regarded as a new way to distinguish patients' stages and assess their condition. Because there are existing fitting errors, the interval of the mean $\langle x_k \rangle$ in each state can be calculated as follows:

$$[x_k^l, x_k^u] = \left[\langle x_k \rangle - \frac{1}{N_k} \sum_{i=1}^{N_k} \mathrm{err}_k^i, \langle x_k \rangle + \frac{1}{N_k} \sum_{i=1}^{N_k} \mathrm{err}_k^i \right]$$

where err_k^i is the fitting error of node i in state k. Therefore, the three intervals in CHB, LC, and HCC are [0.4194, 0.5584), [0.4011, 0.4749], and (0.1353, 0.4292], respectively. We can use these as the diagnosis criteria for patients with long-term HBV infection. Although the average test results of a patient may belong to more than one interval, the state of the patient can be determined by the patient's unique characteristics. For example, in the LC state, patients will experience hypersplenism during the decompensation period, resulting in the decrease of red blood cells (RBCs), white blood cells (WBCs), and PLT. Since more than 70% of HCC patients have a high serum concentration of AFP, we can discern patients with HCC versus other diseases by means of the AFP. To compare our method with physician diagnoses, we re-collected the blood test data of 79 patients, including 19 cases of mild or moderate CHB, 30 cases of decompensated LC, and 30 cases of HCC (the test set is listed in Appendix A). We randomly selected 45 cases (15

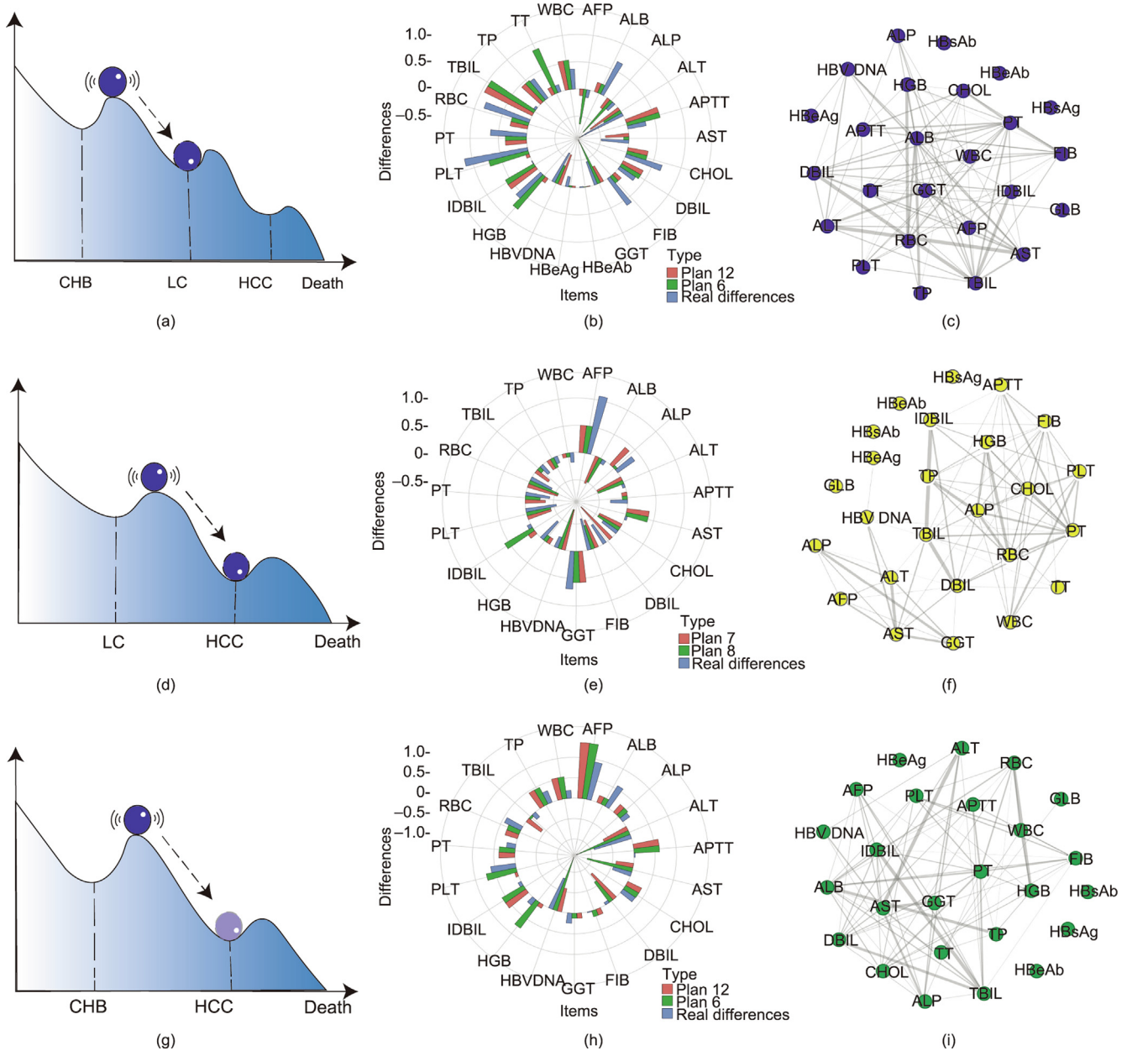

Fig. 5. Critical states. (a) The peak of the phase transition graph shows a critical state, fibrosis, in patients (dark blue ball), which may develop into LC in the future if treatment is not provided. (b) By setting several schemes to perturb items, we compared the tendency of each item with differences in the states of CHB and LC. Blue bars show the difference in an item in the CHB and LC states (the other bars represent tendencies in different plans). As shown, they have the same signs. (c) We constructed a possible network in the critical state. (The method is provided in Section S2.1 in Appendix A.) (d–i) The remaining two situations involving precancerous lesions are similar.

for each disease) to create three dissimilar online questionnaires with the same difficulty level[†]. We invited 218 physicians from different hospitals in hepatobiliary surgery, infection, gastroenterology, or other departments to participate in the survey. Each physician filled out a questionnaire at random.

Due to the similar sample sizes of the three diseases in the test set, we can evaluate the efficacy of the method using the macro-averaged precision and macro-averaged recall. As illustrated in Fig. 4(a), the macro-averaged precision of our method, functional resilience, is 84.74%, whereas the macro-averaged precision of physicians' experience without imaging or biopsy assistance in identifying the three diseases is 55.63%. Similarly, the macro-averaged recall of our method versus that of physicians' experience is 84.39% and 55.45%, respectively. To equalize the impact of precision and recall, we evaluate the efficacy of the two methods using the F1-score. In comparison, the F1-score of our method is 84.50%, which is significantly higher than physicians' experience without imaging or biopsy assistance. Therefore, our method is more accurate than physicians' experience.

According to the American Association for the Study of Liver Diseases (AASLD) Practice Guidance, CHB is diagnosed when HBsAg is positive for more than six months, serum HBV DNA is higher than 20 000 IU·mL^{-1} (lower values of 2000–20 000 IU·mL^{-1} are frequently observed in HBeAg-negative CHB), and there is persistent or intermittent elevation in ALT or aspartate transaminase levels

[†] The links to the online questionnaires are https://www.wjx.cn/vj/wi7wVdE.aspx, https://www.wjx.cn/vj/PnjzmtM.aspx, and https://www.wjx.cn/v j/YzgHzaA.aspx.

[46]. Therefore, pertinent blood tests are performed on patients seeking medical care. Since portal hypertension, whose independent predictors are the diameter of fibrous septa and the size of nodules, is an early clinical sign of liver cirrhosis progression [47,48], physicians commonly recommend patients to undertake additional imaging tests for LC. If the patient self-reports a family history of liver cancer, or if the patient's alpha-fetoprotein exceeds 200 $g{\cdot}L^{-1}$ for more than eight weeks or 400 $g{\cdot}L^{-1}$ for more than four weeks during follow-up, the physician will usually recommend imaging or a liver biopsy to determine whether there is a space-occupying lesion. Although a biopsy has the potential to establish an accurate diagnosis in a timely manner, the AASLD does not recommend its routine use. This is because a biopsy carries the risk of hemorrhage and tumor dissemination, as well as the possibility that a negative result is due to the inability to obtain tissue that is representative of the nodule, as opposed to a nodule that is genuinely benign [33]. In general, the order of imaging used by physicians is ultrasound, CT, contrast-enhanced CT, MRI, and dynamic contrast-enhanced MRI. At the time of diagnosis or follow-up, all hepatitis B patients should undergo at least one imaging examination and blood tests. If the disease is complex, it may be necessary to conduct multiple imaging investigations.

In contrast, according to our method, physicians can make clinical decisions with 84.74% precision from blood tests alone. Indeed, our method may not be able to distinguish an ambiguous state precisely, and the calculated indicators may fall in the range of multiple diseases. A prominent example is HCC with a negative serum AFP (< 20 $ng{\cdot}mL^{-1}$). In China, about 30%–40% of HCC patients are negative for serum AFP [49]. At this time, a single imaging test, such as a CT or MRI, will be sufficient to corroborate the patient's diagnosis. Table 1 lists the cost of various routine examination methods for CHB, LC, and HCC. Considering the case of HCC, international guidelines state that HCC diagnosis depends on particular radiological findings using CT or MRI scans, as well as histopathological examination. Thus, a patient may undergo laboratory testing, ultrasound, CT scan, and MRI or biopsy before diagnosis. As shown in Figs. 4(b) and (c), without health insurance, a patient would have to pay the equivalent of a minimum of 274.62 USD, not including the cost of treatment, for testing alone. Under the same circumstances, the patient would have to spend at least 2692.00 USD in the United States. Although medical insurance can reimburse part of this cost, the part that patients need to pay for themselves will generally still be a considerable financial burden to the family. In contrast, using our approach, a patient can receive an overview of their liver and an HCC diagnosis for as little as the equivalent of 130.49 USD in China or 417.00 USD in the United States through blood tests. In a situation with CHB or LC, similar outcomes can be found. Compared with usual diagnostic procedures, our method could save at least 30 USD equivalent per visit for most Chinese patients or at least 400 USD per visit for most American patients. This would add up to savings of at least 10.5 billion USD yearly on a global scale. Therefore, our method is cost-effective and can be employed in areas with limited medical resources, making the investigation of diseases associated with HBV easier.

3.5. Phase transition and critical state discovery

In the process of chronic HBV infection, patients with liver disease will not only experience ACLF or death but also encounter phase transitions from the CHB to the LC state and then to the HCC state, or directly from the CHB to the HCC state Fig. 5. During these transitions, there are critical states of liver fibrosis and hepatocellular precancerous lesions that are controllable and even reversible (Figs. 5(a), (d), and (g)). However, patients' failure to perceive fibrosis and precancerous lesions in time, due to a lack of symptoms, gives rise to the development of the diseases. To identify signs of the critical states, we can explore and predict them through the network structures of CHB, LC and HCC, and the dynamics of Eq. (3)

With attention, the behavior of a small part of the network affects the whole system in a nonlinear way. Next, we established several plans to simulate the deteriorating trends in a patient with CHB that transitions into LC or HCC, or a patient with LC that transitions into HCC. According to the different plans (Section S2.1 in Appendix A), the simulations for each situation were solved using a fourth-order Runge-Kutta stepper (MATLAB function ode45). We compared the difference in the test results between different states to determine an optimal plan with a similar tendency. When the test items reach the corresponding values, the patient's condition is deteriorating and may transition to the next state in the future.

Table 2 provides the pivotal factors and their critical ranges under different conditions. For example, in a case with a critical status between CHB and LC, the patient has CHB that has already progressed to liver fibrosis, which has a hazardous tendency to become LC in the future when the patient's test results for these 12 items reach the corresponding values (Fig. 5(b)). In addition, the possible network structure of the fibrosis state has three isolated nodes, which means that the patient's HBsAg, HBsAb, and HBeAb have the same results and do not have correlations with the other items. Its network sparsity is between the networks of the CHB and LC. The remaining two situations about precancerous lesions are similar. In addition, the robustness of the critical networks is lower than those of the CHB, LC, and HCC networks; that is, the critical networks are more vulnerable than the networks before the transitions (see Fig. S4 in Appendix A).

Table 2
Pivotal items and their critical conditions in the phase transitions between HBV-related diseases.

The critical conditions of the phase transition	Items	Ranges
Critical conditions of the phase transition from CHB to LC	RBC	$<4.5 \times 10^{12}\ L^{-1}$
	WBC	Abnormal
	Cholesterol (CHOL)	Abnormal
	TBIL	$>34\ \mu mol{\cdot}L^{-1}$
	DBIL	$>8\ \mu mol{\cdot}L^{-1}$
	IDBIL	$>17.1\ \mu mol{\cdot}L^{-1}$
	Total protein (TP)	$<65\ g{\cdot}L^{-1}$
	Albumin (ALB)	$<40\ g{\cdot}L^{-1}$
	Prothrombin time (PT)	>14 s
	Activated partial thromboplastin time (APTT)	Abnormal
	Fibrinogen (FIB)	Abnormal
Critical conditions of the phase transition from LC to HCC	HBV DNA	$\geq 20\ IU{\cdot}mL^{-1}$
	AST	$>40\ U{\cdot}L^{-1}$
	ALT	>0
	ALP	$>110\ U{\cdot}L^{-1}$
	GGT	$>60\ U{\cdot}L^{-1}$
	AFP	$>7\ ng{\cdot}mL^{-1}$
Critical conditions of the phase transition from CHB to HCC	RBC	$<4.5 \times 10^{12}\ L^{-1}$
	WBC	Abnormal
	ALP	$>110\ U{\cdot}L^{-1}$
	GGT	$>60\ U{\cdot}L^{-1}$
	CHOL	Abnormal
	IDBIL	$>17.1\ \mu mol{\cdot}L^{-1}$
	TP	$<65\ g{\cdot}L^{-1}$
	ALB	$<40\ g{\cdot}L^{-1}$
	PT	>14 s
	APTT	Abnormal
	FIB	Abnormal
	AFP	$>200\ ng{\cdot}mL^{-1}$

4. Conclusions and discussion

Our aim with this research was to assess the liver conditions of patients with HBV, reduce the cost of diagnosis, and provide an early warning of liver function deterioration. We described the liver function status under the conditions of CHB, LC, and HCC from a network perspective by constructing networks of 25 items based on the patients' blood tests. We then determined the evolution dynamics of liver function and analyzed the liver function of patients with CHB, LC, and HCC from an analytical standpoint. By arbitrarily deleting links or altering their weights, we simulated the process of chronic HBV infection progressively causing liver dysfunction. Furthermore, we presented pivotal indications and related thresholds of the critical states between CHB, LC, and HCC by combining network structure and dynamics. These findings have significant implications for HBV-related disease-prevention research. When the key test items exceed the threshold, patients may transition between states. Although the morphology of the liver in a critical state is unknown, our results can inspire future research.

In our model, we defined the new measure of functional resilience and found that substantial variation in the functional resilience values of patients in the CHB, LC, and HCC states can be used to diagnose liver disease. Our method has a macro-averaged precision of 84.74%, whereas the macro-averaged precision of physicians' expertise without the assistance of imaging or biopsy to detect these three diseases is only 55.63%, according to our survey. The macro-averaged recall of our method is 84.39%, in comparison with that of physicians at 55.45%. Moreover, the F1-score of our method is 84.50%, which is substantially higher than that of clinicians' experience without imaging or biopsy assistance. In general, our procedure is more precise than physicians' expertise. Therefore, our approach can help primary physicians diagnose HBV-related diseases based on only a few blood samples. By combining the blood tests that patients typically receive, our method can be utilized to diagnose HBV-related diseases and assist clinicians with qualitative and quantitative liver function assessments. With the collection of only a small amount of blood, our method allows physicians to gain an understanding of their patients' condition that can provide a basis for therapy or referral, based on the functional resilience of the liver. For patients with severe malnutrition, prolonged coagulation time, or relatively large tumors, liver function can be known only through blood testing, without requiring liver puncture. From an economic perspective, our strategy may result in savings of the equivalent of at least 30 USD per visit for most Chinese patients and at least 400 USD per visit for most American patients, compared with current diagnostic techniques. A minimum of 10.5 billion USD will be saved yearly on a global scale. At the same time, our method allows clinicians in low- or middle-income nations, especially those in Africa, to examine a patient's liver function using the available blood testing equipment, which will dramatically decrease these countries' medical expenditures for HBV diagnosis. Hence, our method can significantly mitigate personal and national medical economic burdens.

Acknowledgments

This work was supported by National Natural Science Foundation of China (72231008, 72171193, and 72071153).

Compliance with ethics guidelines

Gege Hou, Yunru Chen, Xiaojing Liu, Dong Zhang, Zhimin Geng, and Shubin Si declare that they have no conflict of interest or financial conflicts to disclose.

Appendix A. Supplementary data

Supplementary data to this article can be found online at https://doi.org/10.1016/j.eng.2023.06.013.

References

[1] Lee WM. Hepatitis B virus infection. N Engl J Med 1997;337(24):1733–45.
[2] Mitchell AE, Colvin HM. Hepatitis and liver cancer: a national strategy for prevention and control of hepatitis B and C. Washington, DC: National Academies Press; 2010.
[3] Lavanchy D. Hepatitis B virus epidemiology, disease burden, treatment, and current and emerging prevention and control measures. J Viral Hepat 2004;11(2):97–107.
[4] Qirbi N, Hall A. Epidemiology of hepatitis B virus infection in the Middle East. EMHJ-Eastern Mediterranean Health J 2001;7(6):1034–45.
[5] Kavosi Z, Zare F, Jafari A, Fattahi MR. Economic burden of hepatitis B virus infection in different stages of disease; a report from southern Iran. Middle East J Dig Dis 2014;6(3):156–61.
[6] Li X, Lu J, Hu S, Cheng KK, De Maeseneer J, Meng Q, et al. The primary health-care system in China. Lancet 2017;390(10112):2584–94.
[7] Liu Q, Wang B, Kong Y, Cheng KK. China's primary health-care reform. Lancet 2011;377(9783):2064–6.
[8] WHO. Guidelines for the prevention, care and treatment of persons with chronic hepatitis B infection. Report. Geneva; World Health Organization; 2015.
[9] Shimakawa Y, Njie R, Ndow G, Vray M, Mbaye PS, Bonnard P, et al. Development of a simple score based on HBeAg and ALT for selecting patients for HBV treatment in Africa. J Hepatol 2018;69(4):776–84.
[10] Bruix J, Sherman M; American Association for the Study of Liver Diseases. Management of hepatocellular carcinoma: an update. Hepatology 2011;53(3):1020–2.
[11] Ichikawa T, Saito K, Yoshioka N, Tanimoto A, Gokan T, Takehara Y, et al. Detection and characterization of focal liver lesions: a Japanese phase III, multicenter comparison between gadoxetic acid disodium-enhanced magnetic resonance imaging and contrast-enhanced computed tomography predominantly in patients with hepatocellular carcinoma and chronic liver disease. Invest Radiol 2010;45(3):133–41.
[12] Ginzberg D, Wong RJ, Gish R. Global HBV burden: guesstimates and facts. Hep Intl 2018;12(4):315–29.
[13] Sazzadur Rahman AKM, Javed Mehedi Shamrat FM, Tasnim Z, Roy J, Hossain SA. A comparative study on liver disease prediction using supervised machine learning algorithms. Int J Sci Tech Res 2019;8(11):419–22.
[14] Owjimehr M, Danyali H, Helfroush MS, Shakibafard A. Staging of fatty liver diseases based on hierarchical classification and feature fusion for back-scan–converted ultrasound images. Ultrason Imaging 2017;39(2):79–95.
[15] Khan S, Ullah R, Khan A, Ashraf R, Ali H, Bilal M, et al. Analysis of hepatitis B virus infection in blood sera using Raman spectroscopy and machine learning. Photodiagn Photodyn Ther 2018;23:89–93.
[16] Wang K, Lu X, Zhou H, Gao Y, Zheng J, Tong M, et al. Deep learning radiomics of shear wave elastography significantly improved diagnostic performance for assessing liver fibrosis in chronic hepatitis B: a prospective multicentre study. Gut 2019;68(4):729–41.
[17] Ye Q, Qin L, Forgues M, He P, Kim JW, Peng A, et al. Predicting hepatitis B virus-positive metastatic hepatocellular carcinomas using gene expression profiling and supervised machine learning. Nat Med 2003;9(4):416–23.
[18] Wong GL, Hui VW, Tan Q, Xu J, Lee HW, Yip TC, et al. Novel machine learning models outperform risk scores in predicting hepatocellular carcinoma in patients with chronic viral hepatitis. JHEP Rep 2022;4(3):100441.
[19] Chang TT, Lai CL, Yoon SK, Lee SS, Coelho HSM, Carrilho FJ, et al. Entecavir treatment for up to 5 years in patients with hepatitis B e antigen-positive chronic hepatitis B. Hepatology 2010;51(2):422–30.
[20] Marcellin P, Gane E, Buti M, Afdhal N, Sievert W, Jacobson IM, et al. Regression of cirrhosis during treatment with tenofovir disoproxil fumarate for chronic hepatitis B: a 5-year open-label follow-up study. Lancet 2013;381(9865):468–75.
[21] Lai CL, Wong D, Ip P, Kopaniszen M, Seto WK, Fung J, et al. Reduction of covalently closed circular DNA with long-term nucleos(t)ide analogue treatment in chronic hepatitis B. J Hepatol 2017;66(2):275–81.
[22] Wong GL, Chan HL, Mak CW, Lee SK, Ip ZM, Lam AT, et al. Entecavir treatment reduces hepatic events and deaths in chronic hepatitis B patients with liver cirrhosis. Hepatology 2013;58(5):1537–47.
[23] Wu CY, Lin JT, Ho HJ, Su CW, Lee TY, Wang SY, et al. Association of nucleos(t)ide analogue therapy with reduced risk of hepatocellular carcinoma in patients with chronic hepatitis B: a nationwide cohort study. Gastroenterology 2014;147(1):143–51.
[24] Shim JH, Lee HC, Kim KM, Lim YS, Chung YH, Lee YS, et al. Efficacy of entecavir in treatment-naïve patients with hepatitis B virus-related decompensated cirrhosis. J Hepatol 2010;52(2):176–82.
[25] Wu CY, Chen YJ, Ho HJ, Hsu YC, Kuo KN, Wu MS, et al. Association between nucleoside analogues and risk of hepatitis B virus-related hepatocellular carcinoma recurrence following liver resection. J Am Med Assoc 2012;308(18):1906–13.

[26] Chu CM, Lin CC, Chen YC, Jeng WJ, Lin SM, Liaw YF. Basal core promoter mutation is associated with progression to cirrhosis rather than hepatocellular carcinoma in chronic hepatitis B virus infection. Br J Cancer 2012;107(12):2010–5.
[27] Yang B, Li M, Tang W, Liu W, Zhang S, Chen L, et al. Dynamic network biomarker indicates pulmonary metastasis at the tipping point of hepatocellular carcinoma. Nat Commun 2018;9:678.
[28] White YS, Johnson PJ, Davison F, Williams R. Frequency of hepatic HBV-DNA in patients with cirrhosis and hepatocellular carcinoma: relation to serum HBV markers. Br J Cancer 1990;61(6):909–12.
[29] Neuveut C, Wei Y, Buendia MA. Mechanisms of HBV-related hepatocarcinogenesis. J Hepatol 2010;52(4):594–604.
[30] Artegiani B, van Voorthuijsen L, Lindeboom RGH, Seinstra D, Heo I, Tapia P, et al. Probing the tumor suppressor function of bap1 in crispr-engineered human liver organoids. Cell Stem Cell 2019;24(6):927–43.
[31] DiStefano JK, Davis B. Diagnostic and prognostic potential of AKR1B10 in human hepatocellular carcinoma. Cancers 2019;11(4):486.
[32] Terrault NA, Lok ASF, McMahon BJ, Chang KM, Hwang JP, Jonas MM, et al. Update on prevention, diagnosis, and treatment of chronic hepatitis B: AASLD 2018 hepatitis B guidance. Hepatology 2018;67(4):1560–99.
[33] Marrero JA, Kulik LM, Sirlin CB, Zhu AX, Finn RS, Abecassis MM, et al. Diagnosis, staging, and management of hepatocellular carcinoma: 2018 practice guidance by the american association for the study of liver diseases. Hepatology 2018;68(2):723–50.
[34] Heimbach JK, Kulik LM, Finn RS, Sirlin CB, Abecassis MM, Roberts LR, et al. AASLD guidelines for the treatment of hepatocellular carcinoma. Hepatology 2018;67(1):358–80.
[35] Child CG, Turcotte JG. Surgery and portal hypertension. Major Probl Clin Surg 1964;1:1–85.
[36] Pugh RN, Murray-Lyon IM, Dawson JL, Pietroni MC, Williams R. Transection of the oesophagus for bleeding oesophageal varices. Br J Surg 1973;60(8):646–9.
[37] McCulloch WS, Pitts W. A logical calculus of the ideas immanent in nervous activity. Bull Math Biophys 1943;5(4):115–33.
[38] Sompolinsky H, Crisanti A, Sommers HJ. Chaos in random neural networks. Phys Rev Lett 1988;61(3):259–62.
[39] Amit DJ. Modeling brain function: the world of attractor neural networks [dissertation]. Cambridge: Cambridge University; 1989.
[40] Shalapour S, Lin XJ, Bastian IN, Brain J, Burt AD, Aksenov AA, et al. Inflammation-induced IgA+ cells dismantle anti-liver cancer immunity. Nature 2017;551(7680):340–5.
[41] Wu J, Barahona M, Tan Y, Deng H. Natural connectivity of complex networks. Chin Phys Lett 2010;71(7):078902.
[42] Rosvall M, Bergstrom CT. An information-theoretic framework for resolving community structure in complex networks. PNAS 2007;104(18):7327–31.
[43] Rosvall M, Bergstrom CT. Maps of random walks on complex networks reveal community structure. PNAS 2008;105(4):1118–23.
[44] Barzel B, Liu Y, Barabási AL. Constructing minimal models for complex system dynamics. Nat Commun 2015;6(1):7186.
[45] Baumann F, Lorenz-Spreen P, Sokolov IM, Starnini M. Modeling echo chambers and polarization dynamics in social networks. Phys Rev Lett 2020;124(4):048301.
[46] Terrault NA, Bzowej NH, Chang KM, Hwang JP, Jonas MM, Murad MH; American Association for the Study of Liver Diseases. AASLD guidelines for treatment of chronic hepatitis B. Hepatology 2016;63(1):261–83.
[47] Nagula S, Jain D, Groszmann RJ, Garcia-Tsao G. Histological-hemodynamic correlation in cirrhosis—a histological classification of the severity of cirrhosis. J Hepatol 2006;44(1):111–7.
[48] Kumar M, Sakhuja P, Kumar A, Manglik N, Choudhury A, Hissar S, et al. Histological subclassification of cirrhosis based on histological–haemodynamic correlation. Aliment Pharmacol Ther 2008;27(9):771–9.
[49] Zhao C, Zhou W, Chen W, Zhang C. Clinical significanceof afetoprotein ininitial diagnosis of primary hepatic cancer. J Clin Hepatol 2013;29(9):698–701.